Lessons from snake venom: new insights into the structural and functional aspects of factor V and factor X

Verhoef, D.

Chapter 4

Functional crosstalk between the A- and C-domains of blood coagulation factor V modulates phospholipid binding and cofactor stability

Daniël Verhoef, Gerry A.F. Nicolaes, Roy Schrijver, Pieter H. Reitsma, and Mettine H.A. Bos.

Manuscript in preparation

Abstract

Activated blood coagulation factor V (FVa) is an inherently unstable cofactor that is essential in the conversion of prothrombin to thrombin by factor Xa (FXa). In order to interact with FXa and prothrombin, FVa requires interaction with anionic phospholipid membranes via its two C-domains. Interestingly, the venom of the Australian snake *Pseudonaja textilis* contains a highly stable FVa-like homolog (ptFV) that is known to bind venom-derived FXa in the absence of a membrane surface. Moreover, ptFV has lost the ability to bind membranes, despite structural conservation of the C-domain pair. Here, we have explored the functional relationship between cofactor stability and phospholipid binding by exchanging the C-domains between constitutively active B-domainless human FV (hFV) and ptFV, and expressing, purifying and characterizing the chimeric variants hFV-ptC and ptFV-hC. Differential scanning calorimetry analysis and cofactor activity decay rate experiments revealed that the C-domain exchange adversely affected cofactor stability in ptFV-hC relative to ptFV, yet enhanced the stability of hFV-ptC relative to human FV. Furthermore, surface plasmon resonance analysis showed that the A-domains of human FV enabled phospholipid binding by the C-domains of ptFV. On the other hand, phospholipid binding by the human C-domains was reduced when linked to the A-domains of ptFV. In conclusion, our study has shown functional crosstalk between the A-domain trimer and C-domain pair of FV with regard to anionic phospholipid binding and cofactor stability. These findings provide novel insights into the multi-domain relationships that govern FVa cofactor function.

Introduction

Blood coagulation factor V (FV) is an essential cofactor in the conversion of prothrombin to thrombin, the latter converting soluble fibrinogen into insoluble strands of fibrin that serve to stabilize the platelet-based primary blood clot. The conversion of prothrombin is catalyzed by the prothrombinase complex, which is a macromolecular complex consisting of activated factor V (FVa) and activated factor X (FXa) that assembles on a negatively charged membrane surface in the presence of calcium ions [1]. FV circulates in blood as a 330 kDa single-chain inactive procofactor (domain organization A1-A2-B-A3-C1-C2) and is structurally homologous to blood coagulation factor VIII (FVIII) [2]. Activation of FV proceeds via limited proteolysis of its central B-domain by either (meizo)thrombin or FXa, which results in the removal of inhibitory sequences and exposure of the binding sites for FXa and prothrombin [3-6]. Once activated, the cofactor Va radically increases the catalytic rate of the serine protease FXa towards prothrombin [1].

Binding of FVa to an anionic phospholipid membrane is a prerequisite for productive interactions between the cofactor, FXa and prothrombin as it increases the binding affinity of FVa for FXa to a physiologically relevant concentration and facilitates docking of prothrombin onto the assembled prothrombinase complex [7, 8]. The discoidin-like C-domains of FVa coordinate binding to anionic phosphatidylserine (PS)-containing membranes through hydrophobic and electrostatic interactions between the net-negatively charged phospholipid membrane and the positively charged C-domains [9, 10]. It is generally acknowledged that FVa is anchored onto the phospholipid surface through dedicated phosphatidylserine-binding residues that are located on separate membrane binding loops, or so-called "spikes", which protrude from the base of each C-domain [10-15]. Additional studies indicate that the membrane-bound C-domain pair provides support for the three A-domains of FVa, which are arranged on top of the C-domains and engage with FXa and prothrombin [16-20]. Nevertheless, the exact structural arrangement of the C-domain pair relative to that of the A-domain trimer remains ambiguous [17, 18, 21]. In addition, it remains to be determined whether membrane binding is exclusively governed by the C-domains and/or whether the previously observed crosstalk between the C-domain pair and A-domain trimer may also affect the interaction of FV with an anionic surface [15].

The venom of the Australian snake *Pseudonaja textilis* (*P. textilis*) contains a weaponized homolog of FVa (ptFV) that is constitutively active and is able to bind a FXa homolog found in the same venom (ptFXa) with high affinity in the absence a phospholipid surface [22, 23], unlike any FVa species known to date. In addition, ptFV has been reported to display significantly reduced binding to phosphatidylserine-containing membranes [24]. The multi-domain structure of

ptFV is nonetheless identical to human FVa, as it consists of three A-domains and two C-domains that are organized in a configuration resembling membrane-bound FVa [18, 20, 22, 25]. Previously, we have reported that ptFV is functionally highly stable, as it retains cofactor activity upon extended proteolytic processing by the endogenous enzymatic regulator of FVa activity, activated protein C (APC) [23, 26]. Here we explored the functional relationship between the A-domain trimer and C-domain pair with regard to anionic phospholipid binding and functional cofactor stability. To do so, we swapped the C-domains of constitutively active B-domainless human FV (FV-810)[27] and ptFV and expressed, purified, and characterized the chimeric variants hFV-ptC and ptFV-hC. Our findings suggest that the conformational flexibility of the C-domain pair may be required for high affinity binding to procoagulant membranes, while stabilization of inter-domain contacts between the A-domain trimer and C-domain pair could impair membrane association.

Material and Methods

Materials and Reagents

The peptidyl substrate H-D-Phe-Pip-Arg-pNA (S2238) was obtained from Instrumentation Laboratories (Bedford, MA, USA). All cell culture reagents were from Life Technologies (Carlsbad, CA, USA) except insulin-transferrin-sodium selenite (ITS), which was from Roche (Basel, Switzerland). Small unilamellar phospholipid vesicles (PCPS) composed of 95% or 75% (w/w) hen egg L-phosphatidylcholine (PC) and 5% or 25% (w/w) porcine brain L-phosphatidylserine (PS) (Avanti Polar Lipids, Alabaster, AL, USA) were prepared and characterized as described previously [28]. FV-depleted human plasma and Neoplastine CI Plus 10 prothrombin time (PT) reagent were obtained from Diagnostica Stago (Paris, France). Normal pooled human plasma (NPP) was from Sanquin (Amsterdam, The Netherlands). All functional assays were performed in Hepes-buffered saline (HBS: 20 mM Hepes, 0.15 M NaCl, pH 7.5) supplemented with 5 mM $CaCl_2$, 0.1% PEG8000 and filtered over a 0.2 µm filter (assay buffer).

Proteins

Restriction endonucleases SnaBI, XmaI, and EcoRV were obtained from New England Biolabs (Ipswich, MA, USA). DAPA, human α-thrombin, human prothrombin, and human prethrombin-1 were from Haematologic Technologies (Essex Junction, VT, USA). Recombinant human FXa (hFXa) and venom-derived *Pseudonaja textilis* FXa (ptFXa) were prepared, purified, and characterized as described [26, 29]. Recombinant constitutively active B-domainless human factor V (FV810; hFV), venom-derived *P. texilis* FV (ptFV), and the variant ptFV-SS were prepared, purified, and characterized as described previously [23, 26, 27]. Molecular weights and extinction coefficients ($E_{0.1\%,\ 280\ nm}$) of the various proteins have been reported previously [23, 27]. The molecular weight and the extinction coefficient ($E_{0.1\%,\ 280\ nm}$) of the newly generated hFV-ptC and ptFV-hC chimeras were assumed to be similar to FV810 (216,000 kDa; 1.54) and ptFV (170,000 kDa; 1.25), respectively.

Construction of FV variants

The construction of pED-FV810 and pED-ptFV has previously been described [23, 27]. Constructs encoding for human FV (FV810) comprising the venom-derived *P. textilis* C-domains (ptFV sequence Cys1147-Phe1460; Uniprot: Q7SZN0), designated pED-hFV-ptC, and for ptFV comprising the human C-domain sequence (human full-length FV sequence Cys1907-Tyr2224; Uniprot: P12259), named pED-ptFV-hC, were generated employing splicing by overlap extension PCR. Specific oligonucleotides used to generate hFV-ptC were as follows: forward primer A, 5'-CCAGACCGTATTCTCTACATGCCC-3', encoding for human FV amino acid residues 1665-1673; complementary primer set reverse primer

B, 5-CCAGTCCCATTGGTAATTTACAGTCTCTGTCCATGATAAG-3', and forward primer C, 5'-CTTATCATGGACAGAGACTGTAAATTACCAATGGGACTGG-3', of which in the latter the first 22 bases correspond to human full-length FV cDNA, encoding for residues 1901-1907, and the last 18 bases to residues 1148-1154 in the ptFV cDNA; and reverse primer D, '5-CTTATTCCAAGCGGCTTCGGCCAG-3', encoding for pED-ptFV nucleotides 5654-5677. The resulting DNA fragment was TOPO-cloned (Invitrogen), digested with SnaBI and XmaI, gel-purified, and subcloned into pED-FV810 digested with the same enzymes. To ensure the absence of polymerase-induced errors, the entire modified cDNA was sequenced. The ptFV-hC construct was prepared using the same strategy with the following primers: forward primer A, 5'-GGCATTTGCTGAACATGGGTGGG-3', encoding for ptFV residues 1068-1075; complementary primer set reverse primer B' 5-GTCCCATTGGCATCCTACAATCTTTGTCAATGACAGTAAAG-3', and forward primer C, 5'-CTTTACTGTCATTGACAAAGATTGTAGGATGCCAATGGGAC-3', of which in the latter the first 22 bases correspond to ptFV cDNA, encoding for residues 1139-1146, and the last 19 bases to residues 1907-1913 in the human full-length FV cDNA; and reverse primer D, '5-CTTATTCCAAGCGGCTTCGGCCAG-3', encoding for pED-FV810 nucleotides 5918-5941, and restriction enzymes EcoRV and XmaI.

Expression and purification of FV variants

Transfection of the plasmids encoding FV constructs into baby hamster kidney cells, the selection of stable clones, and the expression and purification of FV810 and ptFV were performed as described previously [23, 27, 30]. The purification procedures of FV variants hFV-ptC and ptFV-hC were similar to those described for ptFV [23]. Protein purity was assessed by SDS-PAGE using pre-cast 4–12% gradient gels under nonreducing and reducing conditions (50mM DTT) using the MOPS buffer system (Thermo Scientific; Waltham, MA, USA) followed by staining with Coomassie Brilliant Blue R-250. For pretreatment with thrombin, FV variants (1000 nM) were incubated with 50 nM α-thrombin in assay buffer for 15 minutes at 37°C.

FV-specific Prothrombin Time (PT)-based clotting assay

The specific extrinsic clotting activity was determined using a modified FV-specific PT-based clotting assay. Purified FV samples were serially diluted in assay buffer supplemented with 0.1% bovine serum albumin (BSA). In a typical assay, 25 µl of FV-depleted plasma was mixed with an equal volume of sample, followed by a 60 second incubation period at 37°C. Coagulation was initiated after the addition of 50 µl PT reagent, and the coagulation time was monitored using a Start4 coagulation instrument (Diagnostica Stago). Reference curves consisted of serial dilutions of normal pooled plasma, and one unit of FV activity corresponds to the amount of FV in 1 ml of normal plasma (~8 µg).

Macromolecular substrate activation

Steady-state initial velocities of macromolecular substrate cleavage were determined discontinuously at 25 °C in assay buffer as described [31]. Briefly, progress curves of prothrombin and prethrombin-1 activation were obtained by incubating phospholipids (75:25 PCPS, 50 μM), DAPA (10 μM), and prothrombin or prethrombin-1 (1.4 μM) with recombinant FV variants (20 nM), and the reaction was initiated with 0.1–1.0 nM of hFXa or ptFXa. The rate of prothrombin or prethrombin-1 conversion was measured as described [32]. Additionally, prothrombin conversion was assayed in the presence of 95:5 PCPS (450 nM –1000 μM final) or 75:25 PCPS (10 nM – 100 μM final) phospholipid vesicles for hFV and hFV-ptC.

Differential Scanning Calorimetry (DSC)

DSC was performed on a Nano DSC instrument (TA Instruments, New Castle, DE, USA). FV protein solutions (0.2 mg/ml) were prepared in HBS and degassed. The volume of both the sample and reference cell was 0.3 ml, and the reference cell contained degassed HBS only. The cells were heated from 10°C to 110°C at a rate of 1°C per minute under a pressure of 3 atmospheres. Evaluation of the DSC curves was performed employing the NanoAnalyze 3.6 software pack (TA instruments).

Thermal FVa cofactor activity decay

Thermal denaturation experiments were essentially performed as described previously [33]. In brief, activation of FV variants (450 nM) with α-thrombin (50 nM) was carried out in assay buffer supplemented with 0.1% BSA for 15 minutes at 37°C. Following the inhibition of α-thrombin by the addition of hirudin (60 nM), the sample was equilibrated at ambient temperature for 15 minutes. Subsequently, the activated FV variants (20 nM) were incubated for 3–30 minutes at 52°C, upon which the thermal reaction was terminated by cooling in ice water. The cofactor activities of hFVa and hFVa-ptC aliquots were assessed at 250, 125, 63, and 31 pM FVa in FV-depleted plasma using the modified FV-specific PT-based clotting assay. Cofactor activities of ptFVa and ptFVa-hC were assessed at concentrations of 5.0, 2.5, 1.3, and 0.6 nM. The dataset was analyzed using the Graphpad Prism 7 software suite.

Surface Plasmon Resonance Analysis

Association and dissociation of FV variants to phospholipid vesicles was assessed by Surface Plasmon Resonance (SPR) analysis employing a Biacore T200 biosensor and a L1 sensor chip (GE Healthcare Life Sciences, Chicago, IL, USA) [34]. Biosensor experiments were performed in freshly prepared HBS that was filtered over an 0.2 μm filter. Phospholipids composed of 100% PC, or PC with either 5%, 10% or 25% (w/w) PS were dried under constant nitrogen flow, dissolved in HBS, sonicated for 5 minutes and homogenized by passing the mix fifteen times over a disposable polycarbonate membrane (pore size 0.1 μm) using an

extruder (Avestin Inc, Ottawa, Canada) as described [35]. L1 sensor chip cleaning, lipid coating, lipid stabilization, and lipid surface equilibration was performed as recommended by the manufacturer. Recombinant FV variants (20–2000 nM) were passed over an 100% PC reference surface (channel 1) and PC surfaces containing 5%, 10%, and 25% PS (channels 2, 3, and 4) in HBS at 18°C with a flow rate of 5 µl/min for 300 seconds. Subsequently, dissociation was monitored for 120 seconds. After each incubation, the lipid surfaces were regenerated three times with 50 mM NaOH for 60 seconds at flowrate of 10 µl/min, followed by HBS for 180 seconds, upon which the lipid surfaces were equilibrated with 1 mg/ml BSA in HBS for 60 seconds. Biosensor curves were corrected for binding to the 100% PC reference channel and corrected for the HBS signal. In addition, baseline values were subtracted prior to analysis. Following each series of FV variant incubations (nine concentrations per variant), the lipid surface of the L1-chip was replaced. The apparent dissociation constant ($K_{d,app}$) for the interaction between FV variants and the anionic phospholipid surface was obtained from the dependence of the steady state binding response (defined as binding at the onset of dissociation) on the concentrations of the FV species using nonlinear regression analysis via the Biacore software package.

Sequence alignment and superposition

Amino acid sequences of human FV (Uniprot: P12259) and *P. textilis* venom FV (Uniprot: Q7SZN0) were aligned employing the ClustalW algorithm for multiple sequence alignment (Vector NTI 11.5 Advance software suite, Thermo Scientific, Waltham, MA, USA). The C-domains were super positioned using the PyMOL Molecular Graphics System (Schrödinger, LLC). The isoelectric point was calculated with the ProtParam tool on the ExPASy server [36].

Results

The C-domains of human and *Pseudonaja textilis* venom-derived FV

Alignment of hFV and ptFV polypeptide amino acid sequences revealed that the C-domains share 59% sequence identity and 73% sequence similarity (**Supplementary Figure 1**). Superposition of the human and ptFV C-domains showed structural conservation of the characteristic discoidin-like fold of the C-domain pair and conservation of all three β-hairpin phospholipid binding loops at the base of each C-domain (**Supplementary Figure 2**) [10, 11, 25]. However, several positively charged residues are non-conserved in the ptFV C1-domain, resulting in a significantly lower isoelectric point for the ptFV C1-domain (pI: 6.77) compared to that of hFV (pI: 9.17). Furthermore, polar amino acid substitutions have occurred at six positions within the ptFV C2-domain, resulting in an increased hydrophilic character of ptFV C2 relative to hFV. Additional clusters of amino acids substitutions are found within some of the ptFV phospholipid binding loops and within two elongated loops (hFV: Ser^{1971}-Val^{1987} and Ser^{2130}-Val^{2146}) that cover the crest of the C1- and C2-domains. These latter structures are considered to form an extended surface that faces the A-domain trimer when FVa is bound to a membrane surface [18, 20, 25]. Taken together, the ptFV C-domain pair is relatively similar to that of hFV, yet marked differences occur within specific regions that have been shown to interact with the A-domain trimer or to contribute to phospholipid binding.

Construction and characterization of chimeric FV variants

To investigate whether the C-domains of ptFV convey enhanced cofactor stability and/or altered phospholipid binding affinities, we exchanged the C-domain coding regions of constitutively active B-domainless human FV (hFV, or FV-810) with those of ptFV, thereby generating the chimeric cofactors hFV-ptC and ptFV-hC (**Figure 1A**). SDS-PAGE analysis demonstrated that the purified chimeric variants hFV-ptC and ptFV-hC migrate similar to hFV and ptFV, respectively (**Figure 1B**, **Supplementary Figure 3**). In addition, both ptFV and ptFV-hC migrated as single chain species under non-reducing conditions upon incubation with thrombin, indicating that the unique A2-A3 domain disulfide linker in ptFV is maintained in ptFV-hC (**Figure 1B**) [23, 26]. Cofactor function was evaluated employing a purified prothrombinase assay using recombinant human FXa (hFXa) in the presence of a saturating concentration of phospholipid vesicles (PCPS, 50 μM), resulting in comparable rates of prothrombin activation for both hFV and hFV-ptC (**Figure 1C**). In contrast, the rate of prothrombin activation was approximately 40-fold lower using ptFV as cofactor for hFXa. This is consistent with previous findings and in part relates to the reduced affinity of ptFV for membrane-bound human FXa [23, 37]. Conversely, cofactor function of ptFV improved 3-fold by exchanging the ptFV C-domains for those of hFV.

We next aimed to establish whether the C-domains of ptFV drive its lipid-independent cofactor function and, if so, can sustain this unique property in the setting of human FV. Cofactor function was therefore assayed in the presence or absence of saturating concentrations of anionic phospholipid vesicles using the lipid-independent substrate prethrombin-1 [23, 26]. When using hFXa and lipids, replacing the human C-domains for those of ptFV reduced prethrombin-1 activation by almost 2-fold, relative to hFV (**Table 1**). On the other hand, prethrombin-1 conversion was significantly enhanced following exchange of the ptFV C-domains for those of hFV. These results show that C-domain-targeted humanization of ptFV cofactor improves its cofactor function towards hFXa. Interestingly, with lipids and ptFXa as protease, no prethrombin-1 activation was observed for hFV, whereas replacement of the human C-domains for those of ptFV resulted in detectable thrombin formation (**Table 1**). In the absence of lipids though, the hFV-ptC chimera did not display cofactor activity for either hFXa or ptFXa. Correspondingly, ptFV displayed no or hardly any loss of cofactor function for ptFXa following introduction of the human C-domains in the presence or absence of lipids (**Table 1**). Furthermore, no gain of function towards hFXa was observed for ptFV-hC. Taken together, these findings indicate that the C-domains affect overall cofactor activity towards human or venom-derived FXa in a lipid-dependent manner, but do not drive lipid-independent cofactor function.

Table 1. Prethrombin-1 Activation

Cofactor Species	**Initial Velocity^**	**Initial Velocity**	**Initial Velocity**	**Initial Velocity**
	hFXa	***ptFXa***	***hFXa***	***ptFXa***
	+ PCPS	***+ PCPS***	***- PCPS***	***- PCPS***
	nM IIα/min/ nM Enzyme	*nM IIα/min/ nM Enzyme*	*nM IIα/min/ nM Enzyme*	*nM IIα/min/ nM Enzyme*
hFV (FV-810)	**78 ± 11**	**0**	**0**	**0**
hFV-ptC	**46 ± 8**	**6 ± 6**	**0**	**0**
ptFV-hC	**14 ± 5**	**191 ± 16**	**0**	**174 ± 34**
ptFV	**2 ± 0**	**215 ± 14**	**0**	**237 ± 28**

The initial velocity of thrombin generation (nM IIα/min/nM Enzyme) was determined as described in 'Materials and Methods'. The mean values ± S.D. of two independent determinations are presented.

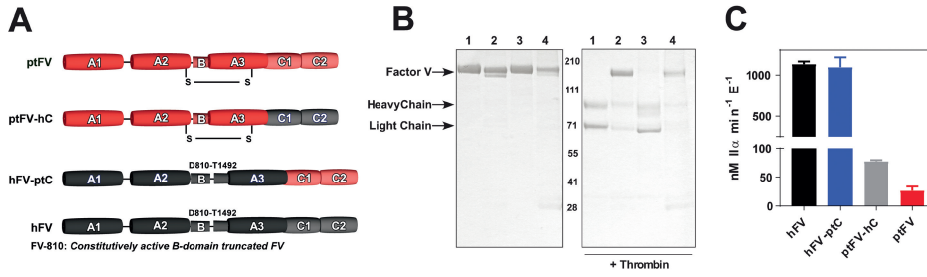

Figure 1. Chimeric FV variants. (***A***) The recombinant FV variants used in this study are shown schematically (ptFV, ptFV-hC, hFV-ptC, and hFV or FV-810); B-domain residues deleted in the human FV variants are indicated. hFV regions are indicated in black and ptFV regions in red. (***B***) Purified proteins (5 µg/lane) were subjected to SDS-PAGE before (left panel) and after treatment with thrombin (right panel) under non-reducing conditions and visualized by staining with Coomassie Brilliant Blue R-250. Lane 1: FV-810; lane 2: ptFV; lane 3: hFV-ptC; lane 4: ptFV-hC. The apparent molecular weights of the standards are indicated. (***C***) Reaction mixtures containing 50 µM PCPS, 10 µM DAPA, 1.4 µM prothrombin, and 20 nM FV variant (hFV or FV-810, hFV-ptC, ptFV, or ptFV-hC) were incubated for 5 min. at 25°C. The reaction was initiated with 0.1 nM hFXa, and thrombin generation was monitored as described in 'Materials and Methods'. The data are the means ± S.D. of two independent experiments.

The C-domains of *P. textilis* FV support cofactor thermostability

To study the cofactor thermostability of each FV variant, we evaluated protein heat capacity by differential scanning calorimetry (DSC). Thermal transition midpoint (T_m) analysis of heat capacity curves revealed a single denaturation event for hFV at 54°C (**Figure 2**). In contrast, ptFV displayed two separate denaturation events, one at 60°C and another at 70°C, pointing to a different and overall higher protein stability compared to hFV (**Figure 2**). As the A2- and A3-domains of ptFV are covalently linked via a disulfide bond that is found in ptFV only [23], we also analyzed the protein heat capacity of a previously characterized ptFV variant that contained serine replacements of the disulfide-forming cysteine pair (ptFV-SS) [26]. While ptFV-SS lacks the A2-A3 connecting disulfide link, we also observed two similar denaturation events, with the second denaturation event occurring at 67°C. This implies that the two sequential denaturation events observed for ptFV and ptFV-SS correspond to separate unfolding events, of which the second event may involve unfolding of the A2-A3 domain region and/or A-domain trimer (**Figure 2**). Interestingly, heat capacity analysis of the chimeric variant hFV-ptC revealed a single denaturation event at 58°C, indicating that the C-domains of ptFV increased cofactor stability when linked to the A-domains of hFV (**Figure 2**). In addition, the thermal transition midpoint of hFV-ptC was preceded by an extended denaturation lag phase, suggesting mitigation of protein unfolding in hFV-ptC. Heat capacity analysis of the chimeric variant that comprised the A-domains of ptFV and the C-domains of hFV did not produce curves that were amenable for thermal transition midpoint analysis.

In order to examine thermal stability of each cofactor in a functional context, we assessed cofactor activity decay rates after incubation at 52°C using a PT-based clotting assay. The central B-domain was removed prior to incubation using thrombin in order to exclude any possible contribution of the B-domain sequence to cofactor stability. By doing so, we were able to confirm the high stability and extended half-life of ptFVa (K <0.001 min^{-1}) relative to human hFVa (K 0.39 ± 0.04 min^{-1}) (**Figure 3**). Similar to the DSC results, hFVa-ptC (K 0.13 ± 0.04 min^{-1}) displayed improved stability and demonstrated a 3-fold prolonged half-life compared to hFVa. On the other hand, the C-domain exchange adversely affected the stability of ptFVa (ptFVa-hC: K 0.73 ± 0.25 min^{-1}), resulting in a more than 30-fold reduced *in vitro* half-life at 52°C relative to ptFVa (**Figure 3**). These findings confirm that the C-domains of ptFV improve cofactor stability in the setting of the human FV A-domains. Conversely, introduction of the human C-domain pair attenuates the thermostability of the ptFV A-domains.

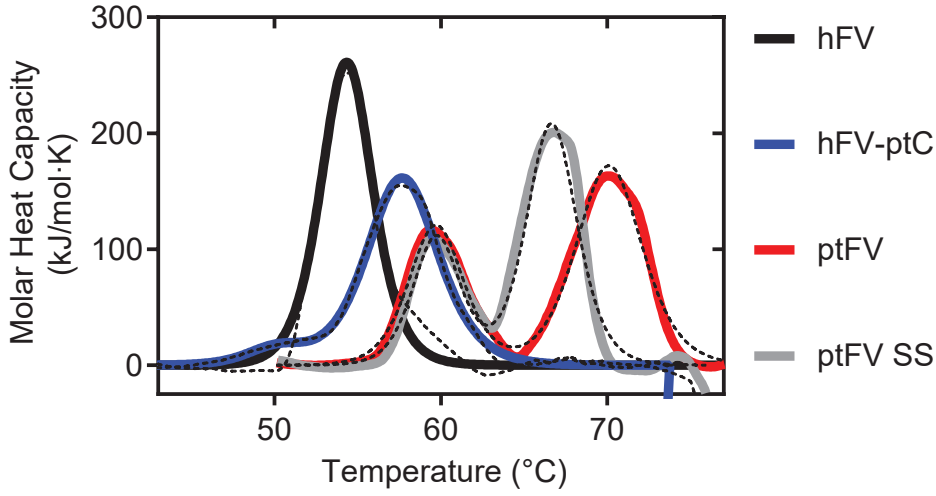

Figure 2. Differential scanning calorimetry. Heat capacity was monitored as described in 'Materials and Methods'. The data were fitted to a two-state model scaled for protein concentration after subtraction of the buffer baseline using the NanoAnalyze software from TA instruments. The derived molar heat capacity is shown for hFV (FV-810, *black*), hFV-ptC (*blue*), ptFV (*red*), or ptFV-SS (*grey*); intermitted lines display raw data curves. The total heat of unfolding (ΔH) was 856 kJ/mol for hFV, 1072 kJ/mol for hFV-ptC, 1569 kJ/mol for ptFV, and 1907 kJ/mol for ptFV-SS. All curves are representative of two similar experiments.

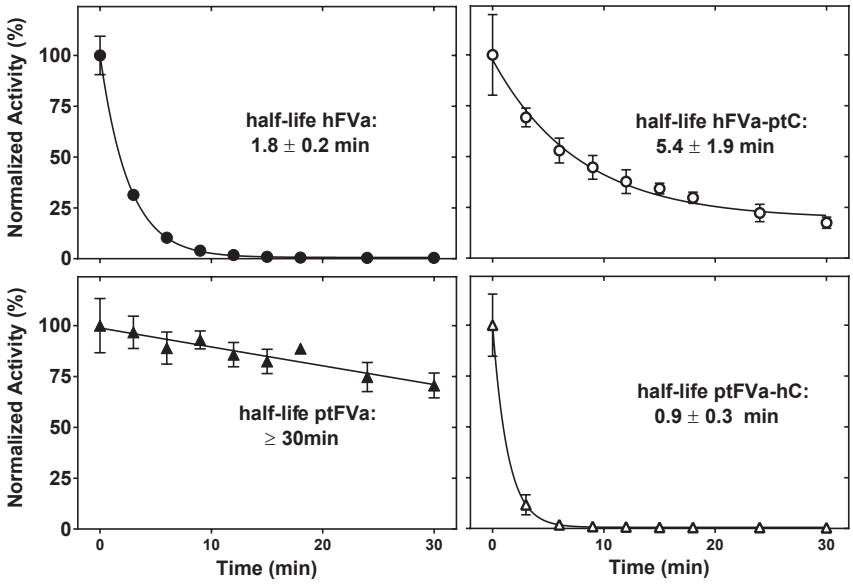

Figure 3. Thermal FVa cofactor stability. Thrombin-activated hFV (FV-810, *closed circles*), hFV-ptC (*open circles*), ptFV (*closed triangles*), or ptFV-hC (*open triangles*) (20 nM) was incubated at 52°C. At the indicated time points, aliquots were processed as described in 'Materials and Methods' and analyzed for FV-specific PT-based clotting activity. The data were normalized to the cofactor activity assessed at the start of the incubation. The cofactor decay rate constants (*K*) were determined by fitting the data to a one-phase decay function by non-linear regression, resulting in the following decay rate constants: hFVa: 0.39 ± 0.04 min^{-1}, hFVa-ptC: 0.13 ± 0.04 min^{-1}, ptFVa: <0.001 min^{-1}, ptFVa-hC: 0.73 ± 0.25 min^{-1}. The corresponding half-lives are indicated in each graph. The data are the normalized means ± S.D. of three independent experiments.

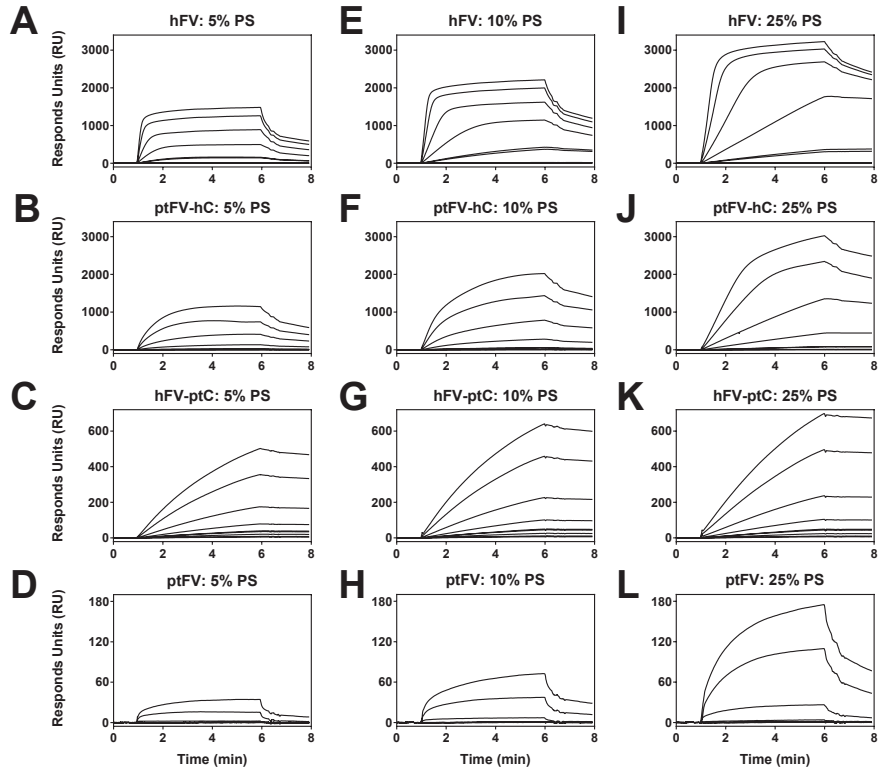

Figure 4. Binding of FV to anionic phospholipid vesicles. The association and dissociation of FV variants (0.02 - 2 μM) to PC phospholipid vesicles containing either 5% PS (***A-D***), 10% PS (***E-H***), or 25% PS content (***I-L***) for hFV (FV-810, ***A-E-I***), ptFV-hC (***B-F-J***), hFV-ptC (***C-G-K***), or ptFV (***D-H-L***) was assessed by SPR as described in 'Materials and Methods'. Cofactor injection started at t = 1 minute and was discontinued at t = 6 minutes. The binding curves were corrected for binding to a control channel coated with 100% PC vesicles (see Supporting **Figure 4)**.

The A-domains of human FV confer lipid binding to the ptFV C-domains

To assess binding of FV to negatively charged phospholipid vesicles, we performed surface plasmon resonance analyses using an L1 chip coated with phospholipid vesicles containing 5%, 10%, or 25% PS (**Figure 4**). Fitting of the phospholipid binding affinity at steady state of hFV revealed an apparent K_d of 1.0 μM for an anionic membrane surface with 5% PS content, and an apparent K_d of 0.5 μM for surfaces with 10% or 25% PS content (**Figure 5**). Binding curves of hFV-ptC, ptFV-hC and ptFV did not display saturation of the binding response at high ligand concentrations (**Figure 4**), precluding regular fitting of the binding constant at steady state. Estimation of their respective binding affinities nonetheless revealed micromolar affinities for both ptFV-hC and hFV-ptC, and millimolar affinities for ptFV (**Figure 5**). While these estimates indicated that ptFV-hC may display an increased affinity towards membranes comprising a higher PS content, this was not observed for hFV-ptC, suggesting reduced phosphatidylserine binding affinity for the ptFV C-domains. These results corroborate the C-domains as the main driving force in the interaction with anionic phospholipids, and confirm that the C-domains of ptFV display reduced lipid binding [24]. Intriguingly, our data also points to a role for the A-domains in mediating phospholipid binding by the C-domains, as the A-domains of human FV enhanced phospholipid binding by the C-domains of ptFV.

The affinity of hFV or hFV-ptC for phospholipid vesicles containing PS was further examined in a functional context by employing a purified prothrombinase assay with hFXa and increasing phospholipid concentrations. Both hFV and hFV-ptC displayed similar prothrombin activation rates in the presence of 25 - 100 μM of phospholipids containing 25% PS (**Figure 1C**). However, hFV-ptC required a 6-fold higher lipid concentration in order to produce half maximal prothrombin conversion rates (**Figure 6A**). Similar findings were obtained at 5% PS content, as hFV-ptC required an approximate 50-fold higher phospholipid concentration in order to generate prothrombin activation rates that were comparable to that of hFV (**Figure 6B**). These results confirmed that the ptFV C-domains displayed reduced affinity towards PS-containing membranes. Nevertheless, the ptFV C-domain pair has re-established the ability to bind to phospholipids in a manner that is conducive to cofactor function when paired with the human A-domain trimer.

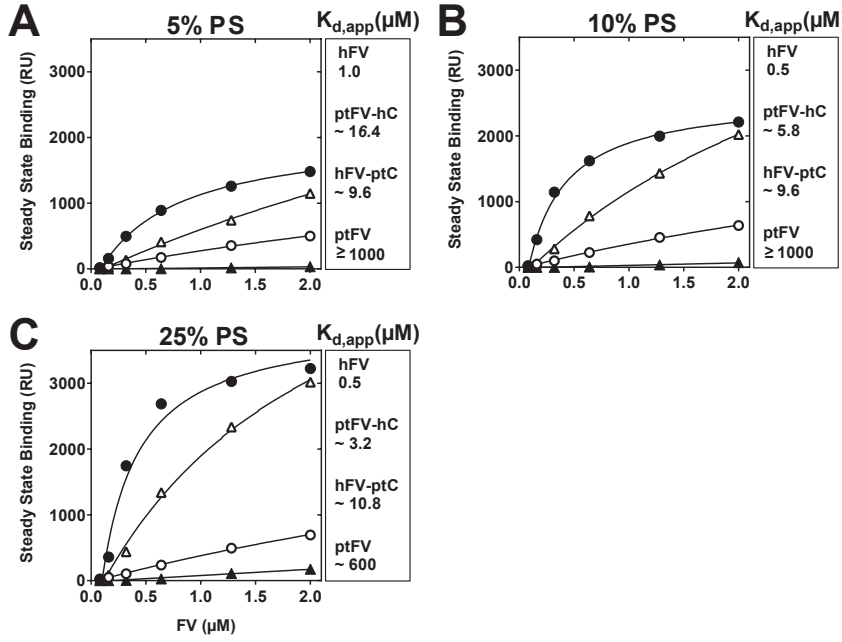

Figure 5. Steady state anionic phospholipid binding affinity. From the anionic phospholipid-FV binding data (**Figure 4)**, the binding response units (RU) at the onset of dissociation were plotted versus the concentrations (0.020-2 μM) of FV. The FV species were hFV (FV-810, *closed circles*), hFV-ptC (*open circles*), ptFV (*closed triangles*) or ptFV-hC (*open triangles*), and the interaction with phospholipid vesicles containing either 5% PS (**A**), 10% PS (**B**) or 25% PS content (**C**) that were coated to an L1 chip was studied employing SPR as described in 'Materials and Methods'. The apparent dissociation constants ($K_{d,app}$) were obtained following nonlinear regression analysis and are presented in the right-hand panels; numbers preceded by the operator (~) indicate estimated affinities; the operator (≥) indicates a low-end estimate.

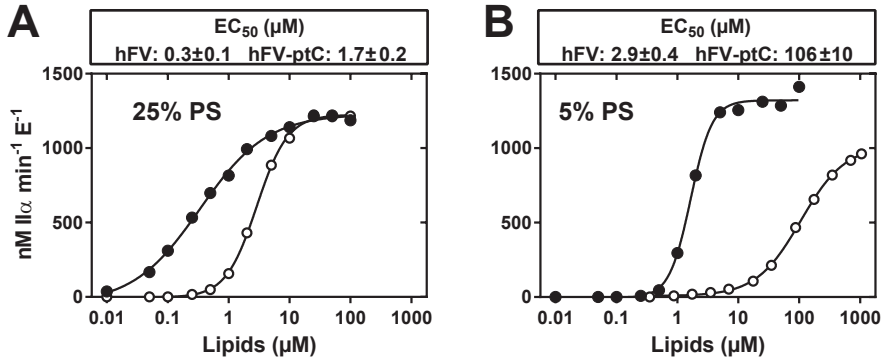

Figure 6. Phospholipid-dependent prothrombin activation. The initial velocity of thrombin generation (nM IIα/min/nM Enzyme) was determined in the presence of 0.1 nM FXa, 1.4 μM prothrombin, 10 μM DAPA and 20 nM hFV (FV-810, closed circles) or hFV-ptC (open circles) at increasing concentrations of phospholipid vesicles containing either 25% PS (***A***) or 5% PS (***B***) as described in 'Materials and Methods'. Lines represent best-fit EC_{50} curves. Insets: best-fit EC_{50} concentrations ± S.D. of the induced fit. All data points represent the means of two independent experiments.

Discussion

Over the past twenty years, the arrangement of the C-domain pair relative to that of the A-domain trimer of FVa and its possible implications to phospholipid binding and cofactor function have been studied systematically [10, 11, 17, 18, 21, 38, 39]. Here, we established the presence of functional crosstalk between the A-domains and C-domains by analyzing chimeric variants of FV that comprise either the A-domains of human FV and the C-domains of ptFV, or vice versa. Specifically, we were able to show that the C-domains of ptFV conferred cofactor stability when linked to the A-domains of human FV while, in turn, the A-domains of human FV improved phospholipid binding by the C-domains of ptFV. However, the absence of a complete and up-to-date crystal structure or NMR ensemble of human FVa restricts a comprehensive rationalization for the observed functional crosstalk between the A-domain trimer and its C-domain pair. Nevertheless, essential clues on the intricate multi-domain relationships that govern cofactor function can be gathered from structural studies on FV and its homolog FVIII.

The first models of the tertiary FV C1/C2 domain structure were generated by Pellequer et al who used the binding domain of galactose oxidase [PDB ID: 1GOF] as structural homolog [38, 40]. These models showed that the C-domains of FV were able to dimerize in a linear or 'head-to-head' fashion to form an extended structure [38]. This configuration was found to be energetically favorable in solution, as hydrophobic residues at the C1/C2 domain interface were buried due to the joining of the two homologous loops that cover the crest of the C1- and C2-domain, here termed apical C1 loop (Ser1971-Val1987) and apical C2 loop (Ser2130-Val2146) (**Supporting Figure 2**). The crystal structures of ceruloplasmin and the FV C2-domain have subsequently been used to construct a multi-domain model of human FVa [10, 39, 41]. This model also includes a linear C-domain arrangement that is connected to the A-domain trimer via a flexible linker connecting the A3 and C1 domains [39]. The crystal structure of APC-inactivated bovine FVa (domain organization A1-A3-C1-C2; FVa_i) was the first to feature a juxtaposed or 'side-by-side' conformation of the C-domains [11]. This arrangement appears to be stabilized by burial of hydrophobic residues at the A3/C1 interface and via extensive electrostatic interactions between the apical C1 loop and the N-terminal β-barrel of the A3-domain [11]. Collectively, depending on the relative orientation of the C-domain pair, the apical C1 loop may associate with the apical C2 loop [39] or the A3-domain [11] (**Supporting Figure 5**). An ensuing Cryo-EM study has shown that the juxtaposed C-domain arrangement represents the FVa-phospholipid binding pose [18]. However, the exact orientation of the membrane-bound C-domain pair relative to that of the A-domain trimer has remained elusive [17, 18]. More recently, Chaves et al applied atomic force microscopy to study activated FV in solution and revealed that the C-domains are, in fact, highly flexible

and able to adopt juxtaposed, linear, and otherwise extended configurations [21]. In other words, the C-domains seem to be in a constant state of rearrangement when FVa resides in solution.

In our current study we have established that the phospholipid binding affinity is inversely correlated to cofactor stability in ptFV. For instance, both DCS and thermal decay experiments clearly showed ptFV to be highly resistant to thermal denaturation, even upon removal of its unique disulfide bond linking the A2 and A3-domains (**Figures 2**,**3**) [26]. On the other hand, SPR experiments revealed that ptFV, of all FV variants tested, displayed the lowest binding affinity for anionic membrane surfaces (**Figures 4**,**5**). Although the ptFV-phospholipid binding was significantly enhanced following exchange of its C-domain pair for that of human FV, this chimeric variant displayed also a significantly shortened half-life during thermal decay experiments, indicating that cofactor stability and membrane binding are mutually exclusive in ptFV. Kinetic analyses have further shown that the ptFV C-domains are of little relevance to its lipid-independent cofactor function, as the chimera ptFV-hC was able to support cofactor function in the absence of phospholipids (**Table 1**). Taken together, these results show that anionic phospholipid binding has been uncoupled from cofactor function in ptFV. This is also reflected by the physical properties of the ptFV C-domains, as membrane binding affinity is potentially attenuated by the neutral isoelectric point of the C1-domain and the more hydrophilic nature of the C2-domain [9, 10, 12-15]. Importantly, sequence alignment revealed a disproportionally high number of amino acid substitutions within sequences that encompass the apical C1 and C2 loops in ptFV (**Supporting Figure 1**). We propose that these alterations serve to restrict dynamical variation in ptFV, effectively stabilizing the cofactor and preventing high affinity phospholipid binding. The full-length structure of ptFV has nevertheless been shown to adopt a juxtaposed C-domain configuration that resembles the human FVa membrane binding pose [18, 20, 25]. We therefore hypothesize that the impaired phospholipid binding affinity of ptFV stems from an inability to arrange its C-domain pair in linear or more extended arrangements, possibly due to reduced avidity between the apical C1/C2 loops and/or enhanced avidity between the A3-domain and the apical C1 loop.

The multi-domain structure of human FVa is recognized as inherently unstable and prone to spontaneous disassociation in the absence of calcium ions. Even so, of all FV variants studied here, hFV (FV-810) displayed the highest overall phospholipid binding affinity following SPR analysis. Interestingly, by linking the ptFV C-domain pair to the human FV A-domain trimer we were able to enhance cofactor stability and simultaneously preserve phospholipid binding (**Figures 2 - 6**). However, the hFV-ptC chimera exhibited significantly slower phospholipid association and dissociation rates, irrespective of vesicle PS content (**Figure 4**) and required 6- to

50-fold higher PS concentrations to achieve maximal prothrombin activation rates (**Figure 6**). These results confirm that the ptFV C-domains are relatively insensitive to PS and potentially less prone to adopt a phospholipid binding pose. In addition, the ptFV C-domains appear to be more stable than their human counterparts. For example, during DSC, we observed a higher thermal transient midpoint for the ptFV C-domain pair at 60°C, while denaturation of the complete hFV cofactor occurred at 54°C. Moreover, both DSC and thermal half-life experiments showed increased stability for both ptFV C-domain comprising cofactors (ptFV, hFV-ptC) relative to the human C-domain comprising cofactors (hFV, ptFV-hC) (**Figures 2**,**3**). Taken together, our observations potentially indicate that the ptFV C-domain pair is less flexible than its human counterpart and could therefore impede multi-domain rearrangements that would otherwise facilitate membrane association and dissociation (**Figure 4**) [15, 21]. Furthermore, our data seem to indicate that the human A-domain trimer can induce C-domain orientations that are conducive to membrane tethering, potentially by enabling the ptFV C-domains to sample more extended configurations. In contrast, the ptFV A-domain trimer was not able to fully support anionic phospholipid binding by the human C-domain pair since the steady state phospholipid binding affinity was reduced for ptFV-hC compared to hFV (**Figures 4**,**5**). Based on these observations we hypothesize that the human A-domain trimer is able to organize its C-domain pair to support selectivity for procoagulant membranes, potentially by reinforcing conformational flexibility of the C-domain pair via allosteric crosstalk between the A-domain trimer and the apical C1 and C2 loops. However, additional biophysical studies are required to substantiate this hypothesis.

Interestingly, conformational flexibility of the C-domain pair appears to be likewise required for high affinity membrane binding in the homologous cofactor VIIIa. For example, computational studies have indicated that flexibility of the FVIII C-domains may be required for the step-wise insertion of the phospholipid binding spikes into procoagulant membrane surfaces [42, 43]. In addition, the relative orientations of C1 and C2, as well as their specific membrane binding properties, have been reported to differ between FV and FVIII [44-47]. As the half-life of FVIIIa is notoriously short, even in comparison to FVa, several studies have been undertaken to improve half-life by introducing covalent links or by increasing hydrophobicity at the A3/C1 or A2/C1 interface [33, 48]. These studies have successfully increased cofactor thermostability, but invariably at the cost of FVIIIa clotting activity [33, 48]. A similar discrepancy was also observed in our study, as the stabile hFV-ptC chimera displayed reduced specific clotting activity while the unstable ptFV-hC chimera displayed increased clotting activity (data not shown). Similarly, a recent study reported decreased cofactor activity and impaired phospholipid binding of a FVIIIa variant that comprised the C1 domain of FV [49]. Conversely, the FV C1-domain was shown to associate more tightly with the A3-

domain of FVIIIa [49], implicating enhanced cofactor stability. In summary, these studies indicate that stabilization of the A3/C1 domain interface may obstruct high affinity phospholipid binding, both in FVIII and FV. Remarkably, sequence conservation of the apical C1 and C2 loop is poor between FV and FVIII, which may imply that these structures might have been molecularly customized to balance cofactor activity versus cofactor half-life during the evolution of the mammalian coagulome.

In conclusion, our study has shown that the A-domain trimer and C-domain pair of FV are functionally linked with regard to anionic phospholipid binding and cofactor stability. These findings provide novel insights into the multi-domain relationships that govern FVa cofactor function and will help to guide future protein engineering strategies.

References

1. Mann, K.G., et al., *Surface-dependent reactions of the vitamin K-dependent enzyme complexes.* Blood, 1990. **76**(1): p. 1-16.
2. Kane, W.H. and E.W. Davie, *Blood coagulation factors V and VIII: structural and functional similarities and their relationship to hemorrhagic and thrombotic disorders.* Blood, 1988. **71**(3): p. 539-55.
3. Suzuki, K., B. Dahlback, and J. Stenflo, *Thrombin-catalyzed activation of human coagulation factor V.* J Biol Chem, 1982. **257**(11): p. 6556-64.
4. Bos, M.H. and R.M. Camire, *A bipartite autoinhibitory region within the B-domain suppresses function in factor V.* J Biol Chem, 2012. **287**(31): p. 26342-51.
5. Schuijt, T.J., et al., *Factor Xa activation of factor V is of paramount importance in initiating the coagulation system: lessons from a tick salivary protein.* Circulation, 2013. **128**(3): p. 254-66.
6. Camire, R.M. and M.H. Bos, *The molecular basis of factor V and VIII procofactor activation.* J Thromb Haemost, 2009. **7**(12): p. 1951-61.
7. Mann, K.G., R.J. Jenny, and S. Krishnaswamy, *Cofactor proteins in the assembly and expression of blood clotting enzyme complexes.* Annu Rev Biochem, 1988. **57**: p. 915-56.
8. Bradford, H.N., S.J. Orcutt, and S. Krishnaswamy, *Membrane binding by prothrombin mediates its constrained presentation to prothrombinase for cleavage.* J Biol Chem, 2013. **288**(39): p. 27789-800.
9. Isaacs, B.S., et al., *A-domain of membrane-bound blood coagulation factor Va is located far from the phospholipid surface. A fluorescence energy transfer measurement.* Biochemistry, 1986. **25**(17): p. 4958-69.
10. Macedo-Ribeiro, S., et al., *Crystal structures of the membrane-binding C2 domain of human coagulation factor V.* Nature, 1999. **402**(6760): p. 434-9.
11. Adams, T.E., et al., *The crystal structure of activated protein C-inactivated bovine factor Va: Implications for cofactor function.* Proc Natl Acad Sci U S A, 2004. **101**(24): p. 8918-23.
12. Nicolaes, G.A., B.O. Villoutreix, and B. Dahlback, *Mutations in a potential phospholipid binding loop in the C2 domain of factor V affecting the assembly of the prothrombinase complex.* Blood Coagul Fibrinolysis, 2000. **11**(1): p. 89-100.
13. Saleh, M., et al., *The factor V C1 domain is involved in membrane binding: identification of functionally important amino acid residues within the C1 domain of factor V using alanine scanning mutagenesis.* Thromb Haemost, 2004. **91**(1): p. 16-27.
14. Peng, W., M.A. Quinn-Allen, and W.H. Kane, *Mutation of hydrophobic residues in the factor Va C1 and C2 domains blocks membrane-dependent prothrombin activation.* J Thromb Haemost, 2005. **3**(2): p. 351-4.
15. Majumder, R., et al., *A phosphatidylserine binding site in factor Va C1 domain regulates both assembly and activity of the prothrombinase complex.* Blood, 2008. **112**(7): p. 2795-802.

16. Autin, L., et al., *Proposed structural models of the prothrombinase (FXa-FVa) complex.* Proteins, 2006. **63**(3): p. 440-50.
17. Lee, C.J., et al., *Proposed structural models of human factor Va and prothrombinase.* J Thromb Haemost, 2008. **6**(1): p. 83-9.
18. Stoilova-McPhie, S., et al., *Defining the structure of membrane-bound human blood coagulation factor Va.* J Thromb Haemost, 2008. **6**(1): p. 76-82.
19. Lee, C.J., S. Wu, and L.G. Pedersen, *A proposed ternary complex model of prothrombinase with prothrombin: protein-protein docking and molecular dynamics simulations.* J Thromb Haemost, 2011. **9**(10): p. 2123-6.
20. Pomowski, A., F.I. Ustok, and J.A. Huntington, *Homology model of human prothrombinase based on the crystal structure of Pseutarin C.* Biol Chem, 2014. **395**(10): p. 1233-41.
21. Chaves, R.C., et al., *Factor Va alternative conformation reconstruction using atomic force microscopy.* Thromb Haemost, 2014. **112**(6): p. 1167-73.
22. Rao, V.S., S. Swarup, and R.M. Kini, *The nonenzymatic subunit of pseutarin C, a prothrombin activator from eastern brown snake (Pseudonaja textilis) venom, shows structural similarity to mammalian coagulation factor V.* Blood, 2003. **102**(4): p. 1347-54.
23. Bos, M.H., et al., *Venom factor V from the common brown snake escapes hemostatic regulation through procoagulant adaptations.* Blood, 2009. **114**(3): p. 686-92.
24. Kumar, S., Stayrook S., Huntington, J.A., Camire, R.M., Krishnaswamy, S., *New Structural Insights into High Affinity Membrane Binding By Coagulation Factor V/Va* Blood, 2014. **124**(21): p. 4216.
25. Lechtenberg, B.C., et al., *Crystal structure of the prothrombinase complex from the venom of Pseudonaja textilis.* Blood, 2013. **122**(16): p. 2777-83.
26. Verhoef D., Y.X., Parthasarathy S., Reitsma P.H., Camire R.M., Bos M.H.A, *Functional implications of the unique disulfide bond in venom factor V from the Australian common brown snake Pseudonaja textilis.* Toxin Reviews, 2013. **33**(1-2): p. 37-41.
27. Toso, R. and R.M. Camire, *Removal of B-domain sequences from factor V rather than specific proteolysis underlies the mechanism by which cofactor function is realized.* J Biol Chem, 2004. **279**(20): p. 21643-50.
28. Higgins, D.L. and K.G. Mann, *The interaction of bovine factor V and factor V-derived peptides with phospholipid vesicles.* J Biol Chem, 1983. **258**(10): p. 6503-8.
29. Verhoef, D., et al., *Engineered factor Xa variants retain procoagulant activity independent of direct factor Xa inhibitors.* Nat Commun, 2017. **8**(1): p. 528.
30. Bradford, H.N., J.A. Micucci, and S. Krishnaswamy, *Regulated cleavage of prothrombin by prothrombinase: repositioning a cleavage site reveals the unique kinetic behavior of the action of prothrombinase on its compound substrate.* J Biol Chem, 2010. **285**(1): p. 328-38.
31. Camire, R.M., *Prothrombinase assembly and S1 site occupation restore the catalytic activity of FXa impaired by mutation at the sodium-binding site.* J Biol Chem, 2002. **277**(40): p. 37863-70.

32. Krishnaswamy, S. and R.K. Walker, *Contribution of the prothrombin fragment 2 domain to the function of factor Va in the prothrombinase complex.* Biochemistry, 1997. **36**(11): p. 3319-30.
33. Wakabayashi, H., A.E. Griffiths, and P.J. Fay, *Increasing hydrophobicity or disulfide bridging at the factor VIII A1 and C2 domain interface enhances procofactor stability.* J Biol Chem, 2011. **286**(29): p. 25748-55.
34. Hodnik, V. and G. Anderluh, *Capture of intact liposomes on biacore sensor chips for protein-membrane interaction studies.* Methods Mol Biol, 2010. **627**: p. 201-11.
35. Wikstrom, A. and J. Deinum, *Probing the interaction of coagulation factors with phospholipid vesicle surfaces by surface plasma resonance.* Anal Biochem, 2007. **362**(1): p. 98-107.
36. Wilkins, M.R., et al., *Protein identification and analysis tools in the ExPASy server.* Methods Mol Biol, 1999. **112**: p. 531-52.
37. Speijer, H., et al., *Prothrombin activation by an activator from the venom of Oxyuranus scutellatus (Taipan snake).* J Biol Chem, 1986. **261**(28): p. 13258-67.
38. Pellequer, J.L., et al., *Homology models of the C-domains of blood coagulation factors V and VIII: a proposed membrane binding mode for FV and FVIII C2 domains.* Blood Cells Mol Dis, 1998. **24**(4): p. 448-61.
39. Pellequer, J.L., et al., *Three-dimensional model of coagulation factor Va bound to activated protein C.* Thromb Haemost, 2000. **84**(5): p. 849-57.
40. Ito, N., et al., *Crystal structure of a free radical enzyme, galactose oxidase.* J Mol Biol, 1994. **238**(5): p. 794-814.
41. Zaitseva I., Z.V., Card G., Moshkov K., Bax B., Ralph A., Lindley P., *The X-ray structure of human serum ceruloplasmin at 3.1 Å: nature of the copper centres.* J Biol Inorg Chem, 1996(1): p. 15-23.
42. Du, J., et al., *Molecular simulation studies of human coagulation factor VIII C-domain-mediated membrane binding.* Thromb Haemost, 2015. **113**(2): p. 373-84.
43. Madsen, J.J., et al., *Membrane Interaction of the Factor VIIIa Discoidin Domains in Atomistic Detail.* Biochemistry, 2015. **54**(39): p. 6123-31.
44. Parmenter, C.D., et al., *Cryo-electron microscopy of coagulation Factor VIII bound to lipid nanotubes.* Biochem Biophys Res Commun, 2008. **366**(2): p. 288-93.
45. Ngo, J.C., et al., *Crystal structure of human factor VIII: implications for the formation of the factor IXa-factor VIIIa complex.* Structure, 2008. **16**(4): p. 597-606.
46. Shen, B.W., et al., *The tertiary structure and domain organization of coagulation factor VIII.* Blood, 2008. **111**(3): p. 1240-7.
47. Gilbert, G.E., et al., *Conservative mutations in the C2 domains of factor VIII and factor V alter phospholipid binding and cofactor activity.* Blood, 2012. **120**(9): p. 1923-32.
48. Wakabayashi, H. and P.J. Fay, *Modification of interdomain interfaces within the A3C1C2 subunit of factor VIII affects its stability and activity.* Biochemistry, 2013. **52**(22): p. 3921-9.
49. Ebberink, E.H., et al., *Factor VIII/V C-domain swaps reveal discrete C-domain roles in factor VIII function and intracellular trafficking.* Haematologica, 2017. **102**(4): p. 686-694.

Supplementary information

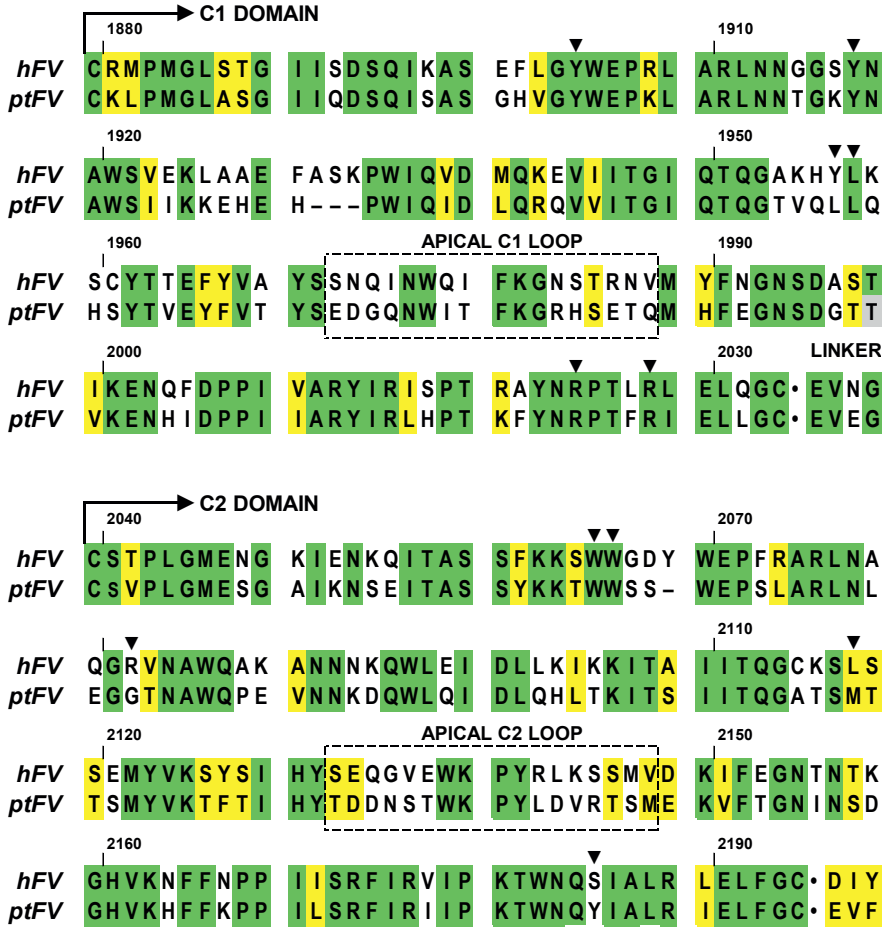

Supplementary Figure 1. Sequence alignment of the C1- and C2-domains of human and ptFV. Alignment of human FV (C^{1879}-Y^{2196}) and ptFV (C^{1117}-F^{1430}) polypeptide chains was performed using the Clustal W algorithm. Color coding: conserved residues (*green*), sequence similarity (*yellow*), non-conserved residues (*clear*). Black triangles denote residues that have been experimentally or structurally implicated in lipid binding [11-15], boxed sequences highlight the apical C1 and C2 loops, the dot indicates the end of the C-domain, and 'LINKER' represents the four residue linker connecting the C1- and C2-domains. Amino acid numbering corresponds to hFV (Uniprot P12259) after subtraction of the 28-residue signal peptide.

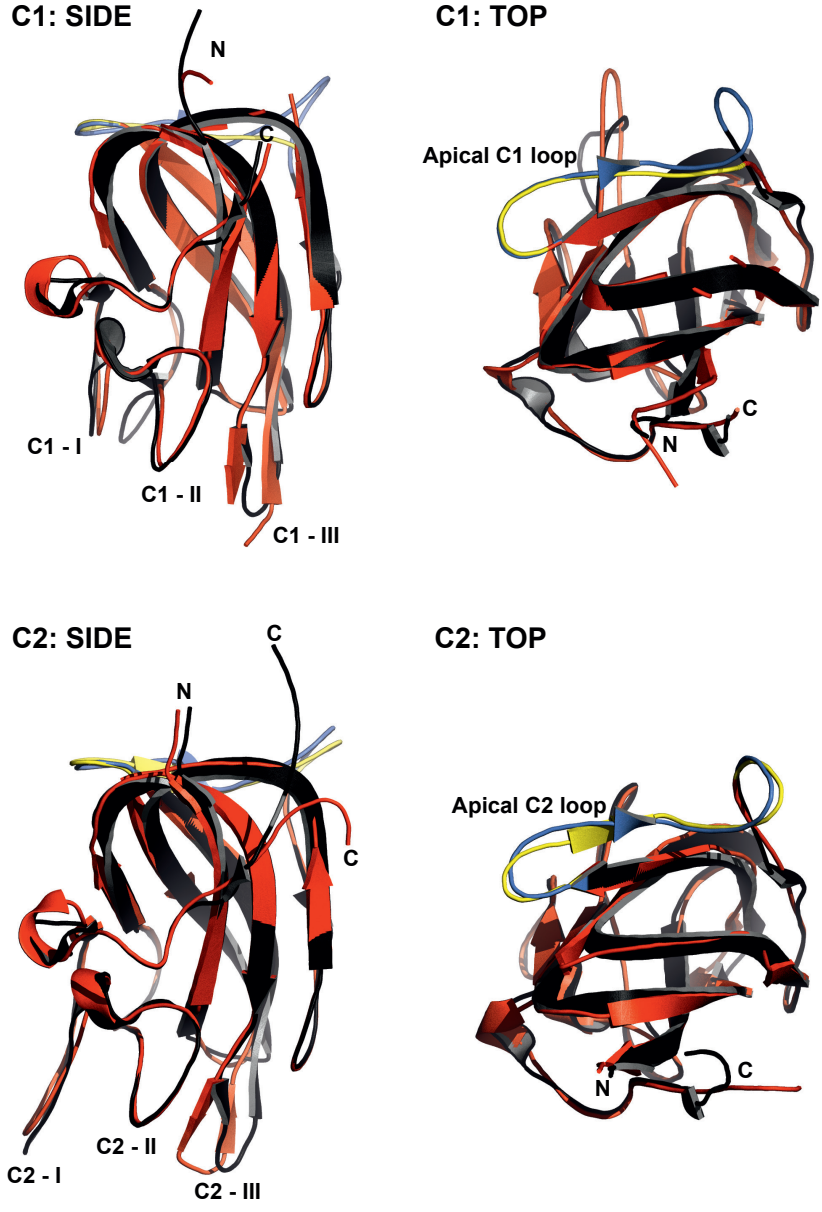

Supplementary Figure 2. Superposition of human FV and ptFV C-domains. The human C-domains (PDB ID 1FV4) and ptFV C-domains (PDB ID 4BXW) [25, 39] were superposed by aligning the structures exclusively to conserved residues. Roman numerals highlight the phospholipid binding spikes. Color coding: hFV (*black*), ptFV (*red*), human apical C1 or C2 loop (*blue*) and ptFV apical C1 or C2 loop (*yellow*). Note: the ptFV apical C1 loop sequence 'R^{1221}-HSET' is not sufficiently resolved in the ptFV crystal structure and is not included in the figure. Visualization and superposition was performed using PyMOL (Schrödinger).

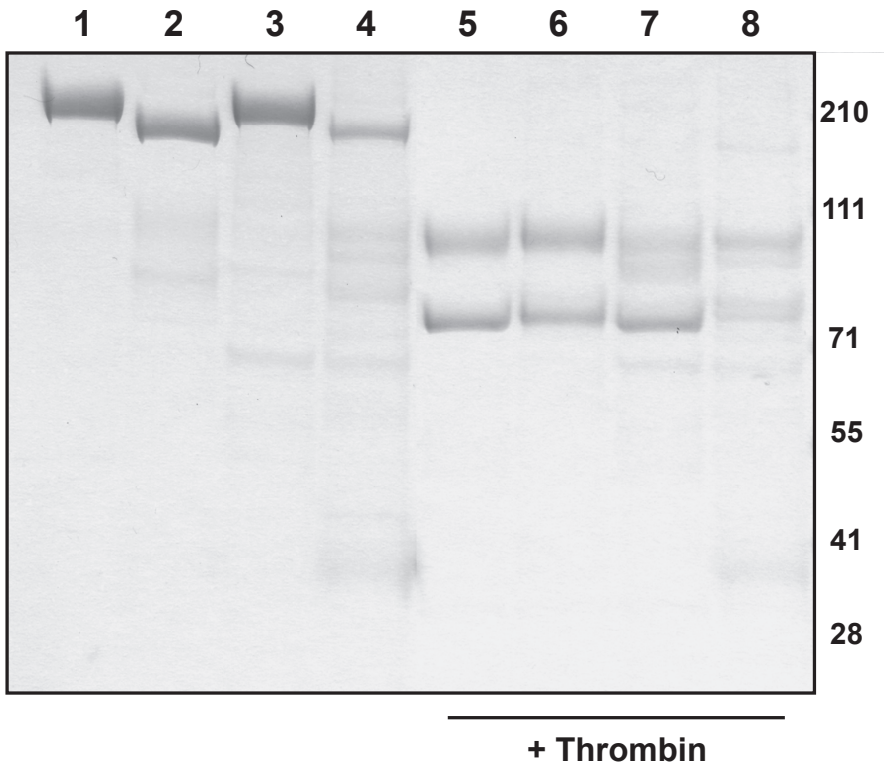

Supplementary Figure 3. Chimeric FV variants. SDS-PAGE analysis of purified proteins (5 µg/lane) before (lanes 1-4) and after treatment with thrombin (lanes 5-8) were subjected to SDS-PAGE under reducing conditions and visualized by staining with Coomassie Brilliant Blue R-250. Lanes 1,5: hFV (FV-810); lanes 2,6: ptFV; lanes 3,7: hFV-ptC; lanes 4,8: ptFV-hC. The apparent molecular weights of the standards are indicated.

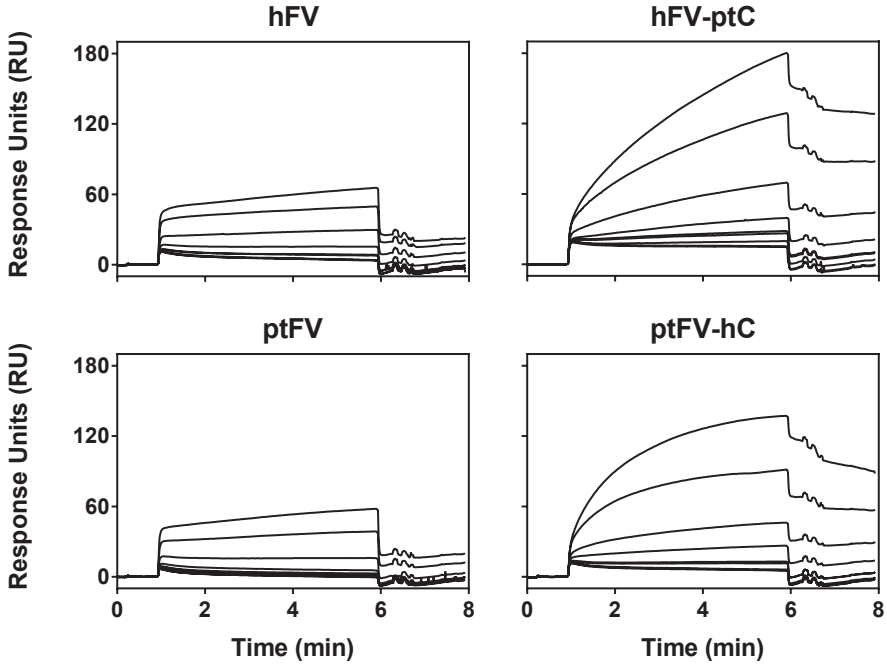

Supplementary Figure 4. Binding of FV to phosphatidylcholine vesicles. Reference association and dissociation phase SPR curves for hFV (FV-810), hFV-ptC, ptFV and pt-FV-hC to an L1 chip coated with phospholipid vesicles containing 100% PC was assessed by SPR as described in 'Materials and Methods'. Cofactor injection started at t = 1 minute and was discontinued at t = 6 minutes. Non-specific binding of FV to 100% PC showed up to 65 response units (RU) of binding at the maximal hFV concentration assessed, 180 RU for hFV-ptC; 140 RU for ptFV-hC, and 40 RU for ptFV.

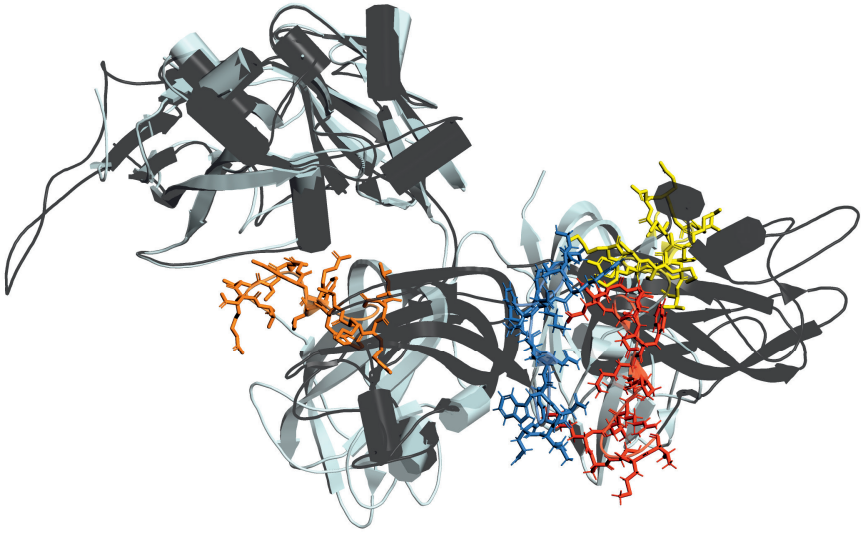

Supplementary Figure 5. The human FVa and bovine FVa$_i$ apical C1 and C2 loops. Superposition of human FVa and bovine FVa$_i$ structures was performed by exclusive alignment of conserved A3-domain residues. The linear C-domain configuration is represented by the model for human FVa (pdb: 1FV4, *dark grey*) [39], and the juxtaposed C-domain configuration is represented by the model for bovine FVa$_i$ (pdb: 1SDD, *light grey*) [11]. The human apical C1 loop (S1971-V1987, *blue*) and apical C2 loop (S2130-V2146, *red*) are highlighted and shown in sticks, the homologous bFVa$_i$ apical C1 loop (*orange*) and apical C2 loop (*yellow*) are shown in sticks as well. The apical C1 and C2 loops are in direct contact with each other while arranged in a linear C-domain configuration (human FVa). In contrast, the apical C1 and C2 loops are spaced apart while arranged in the juxtaposed C-domain configuration (bovine FVa$_i$). Visualization and superposition was performed using PyMOL.


4